A note on wind velocity and pressure spectra inside compact spherical open celled porous microphone windscreens

Feng Niu[1,3], Sipei Zhao[2,*], Xiaojun Qiu[2] and Dong Zhang[1]

[1]MOE Key Laboratory of Modern Acoustics and Institute of Acoustics, Nanjing University, Nanjing, China

[2]Centre for Audio, Acoustics and Vibration, University of Technology Sydney, Sydney, Australia

[3]Division of Mechanics and Acoustics, National Institute of Metrology, Beijing, China

Abstract

Simultaneous measurements of wind velocity and pressure fluctuations are conducted in a wind tunnel to investigate the wind noise source inside compact spherical open celled microphone windscreens. The existing outdoor wind noise models are found to be inadequate to predict the wind noise inside a wind tunnel. This paper proposes a model to predict the interior stagnation pressure, which agrees with the wind noise measured inside the windscreen within a bandwidth, where the exterior turbulence-turbulence interaction pressure overestimates the wind noise level. The shortcomings of the proposed model and other potential sources for wind noise inside porous windscreens are discussed.

Keywords: wind noise, porous windscreen

1. Introduction

Porous microphone windscreens have been widely used to attenuate wind noise in acoustic measurements where microphones are exposed to air flow (Zhao et al., 2018). The wind noise reduction of various porous microphone windscreens has been measured in both wind tunnels and outdoor atmospheric environments.

Raspet et al. (2006) measured outdoor wind noise inside different porous windscreens, and proposed that the upper and lower bounds of wind noise spectra inside spherical porous windscreens were the stagnation pressure and the turbulence-turbulence interaction pressure, respectively. In a further study, the theory was extended from the inertial region to the source region in the lower frequency range, and outdoor measurements with a diverse range of windscreen sizes were analyzed to validate the theory (Raspet et al., 2008). It was concluded that the sum of the turbulence-turbulence and mean shear-turbulence interaction pressures were the lower limit of wind noise that can be achieved by a perfect compact windscreen (Raspet et al., 2008).

In addition to the abovementioned outdoor measurements, wind tunnel experiments have also been conducted to study wind noise inside porous windscreens by many researchers. Based on a series of wind tunnel measurements, Wang et al. (2012) showed that the wind noise reduction increased with the windscreen diameter. Lin et al. (2014) measured the wind noise reduction of various windscreens in a wind tunnel and found their performance to be similar at wind speeds lower than 1.5 m/s. Alamshah et al. (2015) found that the wind noise spectra measured in a small wind tunnel are constant in the lower frequency region but drop off quickly in the higher frequency region. The wind noise spectra inside porous windscreens measured in wind tunnels have been shown to be much different from that measured outdoors (Alamshah et al., 2015; Raspet et al., 2006). However, no theoretical analysis on the noise source based on the measured flow velocity inside compact windscreens within wind tunnels has been found.

In this paper, the wind velocity and pressure spectra are simultaneously measured to investigate the source of wind noise inside a porous windscreen in a wind tunnel. A theoretical model is proposed to describe the wind velocity spectra inside porous windscreens, where both the wind velocity and Reynolds number are much smaller than that outside of the windscreen. Based on the proposed wind velocity spectrum model, the interior stagnation pressure inside the windscreen is calculated. In addition, the exterior stagnation pressure and the turbulence-turbulence interaction pressure are

calculated based on the velocity spectrum measured outside of the windscreen. The calculations are compared with the measurement results with detailed discussions.

2. Theoretical models

2.1 Existing models

To predict the wind noise inside porous microphone windscreens in outdoor measurements, Raspet et al. (2008) employed the von Karman-type model (Eq. (1)) to fit the wind velocity spectrum measured outside windscreens.

$$F(k)=\frac{C}{\left[1+(k\lambda)^2\right]^{5/6}} \tag{1}$$

where C and λ are the fitting constants, k is the turbulence wavenumber in the direction of flow. Based on the fitting constants (C and λ) in Eq. (1), the stagnation pressure (F_{pps}) and the turbulence-turbulence interaction pressure (F_{ppt}) were predicted in Eqs. (2) and (3), respectively (Raspet et al., 2008).

$$F_{\mathrm{pps}}(k)=\frac{\rho^2U^2C}{\left[1+(k\lambda)^2\right]^{5/6}}+\frac{1.451C^2}{\lambda\left[1+0.1129(k\lambda)^2\right]^{5/6}} \tag{2}$$

where ρ and U are air density and the mean flow speed, respectively.

$$F_{\mathrm{ppt}}(k)=\frac{0.811C^2}{\lambda\left[1+0.1792(k\lambda)^2\right]^{7/6}} \tag{3}$$

Raspet et al. (2008) compared the predicted pressure spectra in Eqs. (2) and (3) with the outdoor wind noise, and found that the stagnation pressure in Eq. (2) agreed well with the wind noise measured by an unscreened microphone. The turbulence-turbulence interaction pressure in Eq. (3) was found to agree with the wind noise measured inside 0.6 m and 1.0 m diameter windscreens, which represent the lower limit of the wind noise inside compact porous windscreens (Raspet et al., 2008). It is noteworthy that the predictions were based on fitting the von Karman-type model in Eq. (1) to the velocity spectrum measured outside of the windscreens. However, the presence of the porous windscreen can suppress the wind speed dramatically, leading to much lower wind velocity and smaller Reynolds number inside the windscreen, where the von Karman-type model in Eq. (1) is not suitable (Pope, 2000). To better fit the wind velocity spectrum inside of the porous windscreen, a new model is proposed.

2.2 Proposed model

It has been known that turbulence spectra can be divided into three regions: the energy-containing range (referred as the source region by Raspet et al., (2008)), the inertial range and the dissipation range (Pope, 2000). The von Karman-type model (Eq. (1)) was a combination of the energy-containing range and the inertial range, which agreed well with the velocity spectra in fully developed turbulent flows with a high Reynolds number (Pope, 2000). However, the inertial range cannot be observed when the Reynolds number is small, where the energy-containing range overlaps the dissipation range (Pope, 2000).

For the air flow in wind tunnels, both the mean wind speed and the turbulent velocity fluctuations inside porous windscreens are dramatically reduced due to the presence of the windscreen. In addition, the viscous forces are increased by the friction between the air flow and the porous material, leading to a small Reynolds number and hence the absence of the inertial range. Following a similar approach in Zhao et al. (2017), a velocity structure function model that combines the energy-containing range and the dissipation range is proposed, i.e.,

$$S(r)=\frac{\varepsilon}{15\nu}\frac{r^2}{\left[1+\left(r/r_0\right)^2\right]} \tag{4}$$

where r is the separation distance between two spatial locations, $r_0=\left(30\nu/\varepsilon\right)^{1/2}u_0$ denotes the transition from the energy-containing range to the dissipation range, u_0 is the root-mean-square value of the velocity fluctuations, $\varepsilon=15\nu\left\langle\left(\partial u/\partial x\right)^2\right\rangle$ is the energy dissipation rate, and ν = 1.5 × 10^{-5} m^2s^{-1} is the kinematic viscosity of air (Pope, 2000). When r >> r_0, Eq. (4) approaches the velocity structure function in the energy-containing range, i.e., $S(r)=2u_0^2$, while for r << r_0, Eq. (4) approaches the velocity structure function in the dissipation range, i.e., $S(r)=\frac{\varepsilon}{15\nu}r^2$ (Monin and Yaglom, 1965).

The velocity spectrum can be obtained from the structure function in Eq. (4) following the procedure in Lohse and Muller-Groeling (1995), namely,

$$F(k)=Ae^{-kr_0} \tag{5}$$

where A = $(30\nu/\varepsilon)^{1/2}u_0^3/\pi$ is a constant for a specific turbulent flow. It can be seen from Eq. (5) that in the energy-containing range (kr_0 << 1), the velocity spectrum approaches

a constant that is independent of wavenumber, which is consistent with the von Karman-type model for $k\lambda << 1$ in Eq. (1). In the dissipation range ($kr_0 >> 1$), however, the velocity spectrum shows an exponential decay, which falls off much faster than the von Karman-type model.

Due to the weaker turbulence inside of the windscreen compared to that outside, the interior turbulence-turbulence interaction and mean shear-turbulence interaction pressure are negligible, and only the interior stagnation pressure is calculated based on the simple one-dimensional model i.e., (Raspet et al., 2006)

$$F_p(k) = \rho^2 U^2 F(k) = A\rho^2 U^2 e^{-kr_0} \tag{6}$$

where $F(k)$ is the velocity spectrum in Eq. (5), and the constants A and r_0 can be obtained by fitting Eq. (5) to the velocity spectrum measured inside the porous windscreens.

3. Experiments and discussions

3.1 Experimental setup

Simultaneous measurements of velocity and pressure fluctuations were performed in a small anechoic wind tunnel (Niu et al., 2017) to investigate the wind noise source inside porous windscreens. The experimental setup is illustrated in Fig. 1(a), and Fig. 1(b) shows the mounting of a B&K 4939 microphone and the hot-wire probe of a DANTEC Dynamics MiniCTA 54T42 anemometer. The distance between the microphone and the hot-wire probe was approximate 5 mm. Please note that both the hot-wire probe and the microphone were placed in a small tube structure to protect the hot-wire probe from damaging when inserting to the porous windscreens, as depicted in Fig. 1(b). The effect of the small tube structure on the measurements is discussed below.

Figures. 1(c) and 1(d) show the photos of the experimental setup both with and without the porous windscreen (B&K UA-0237). The diameter of the open cell porous windscreen is 90 cm, but the material and porosity are not clear. In the measurements, the signals from both the hot-wire anemometer and the microphone were captured by a B&K 3560D Pulse Analyser. The velocity and pressure were measured without the windscreen first, and then the windscreen was installed and the velocity and pressure inside the porous windscreen were measured.

The signals were recorded for 60 s (long enough to obtain smooth spectra at frequencies down to microphone cut-off frequency (4 Hz)) with a sampling rate of 8192

Hz. The *pwelch* function in MATLAB was used to calculate the velocity and pressure spectra with the Welch method, where the number of Fast Fourier Transform (FFT) and overlap were 8192 and 50%, respectively. The measurements were repeated three times, but the results were found to be almost the same, hence only the results for one round is shown here for brevity.

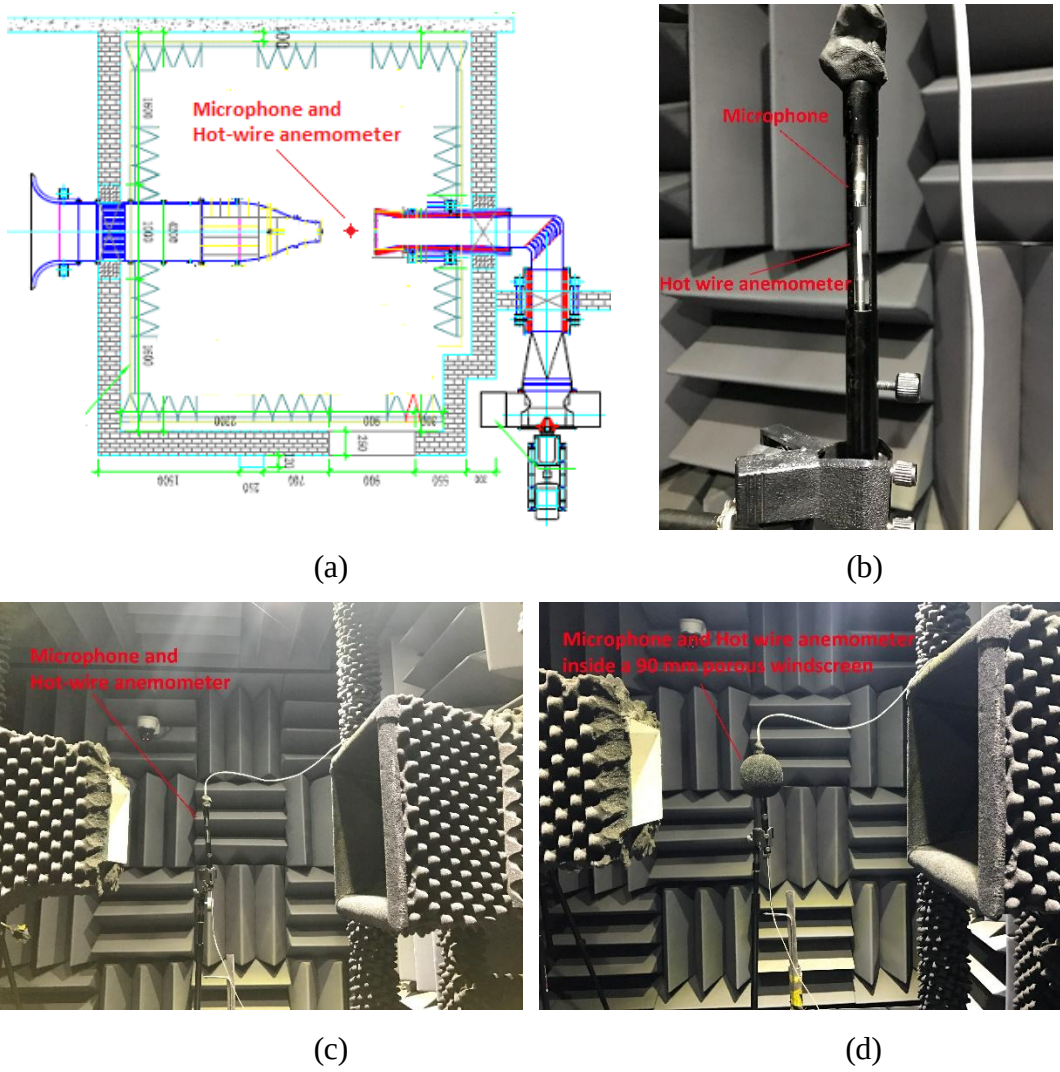

(a) (b)

(c) (d)

Fig. 1. (Color Online) (a) Diagram of the experimental setup; (b) mounting of the microphone and hot-wire probe; and photos of the experimental setup (c) without and (d) with a 90 mm diameter porous microphone windscreen.

3.2 Results and discussions

Figure 2 compares the von Karman-type model in Eq. (1) and the proposed velocity spectrum model in Eq. (5) with the velocity spectra measured both with and without the porous microphone windscreen, at the mean wind speed of 5 m/s. The von Karman-type

model is found to be a good fit for the velocity spectrum measured without the porous windscreen in Fig. 2(a), with the fitting constants C = 0.012 and λ = 0.016. The transition frequency between the energy-containing range and the inertial range can be calculated as $f = 2\pi U/\lambda$ = 50 Hz. In the energy-containing range, both the von Karman-type model and the proposed model are consistent with the measurement results as they are essentially identical. In the inertial range above 50 Hz, the conventional −5/3 power law is clearly observed.

In contrast, the velocity spectrum inside the porous windscreen in Fig. 2(b) decays much faster than the −5/3 power law, which is consistent with the proposed exponential decay model. Comparing Figs. 2(a) and 2(b) shows that the inertial range is dissipated into the dissipation range due to the presence of the porous windscreen. The fitting constants of the proposed model in Fig. 2(b) are $A = 4\times10^{-5}$ and r_0 = 0.02, indicating a transition frequency of $f = 2\pi U/r_0$ = 40 Hz, which is close to the tranistion frequency of 50 Hz for the velocity spectrum measured without the windscreen. The measured velocity spectrum departs the proposed model above 300 Hz as the measured velocity spectrum flattens to the background noise floor. The sharp peaks at 350 Hz and above should be caused by the rotor vibration of the compressor.

It is noteworthy that a broadband peak (between 20 and 60 Hz) near the transition region is noticeable in the measured velocity spectrum in Fig. 2, which can also be observed in the wind noise pressure spectra in Fig. 3. Similar local maxima between 10 Hz and 100 Hz in wind noise spectra were also observed in the measurements by Wang et al. (2012) and Alamshah et al. (2015) in the anechoic wind tunnel of the University of Adelaide. The exact reason is unclear yet and needs further investigation, which is out of the scope of this study.

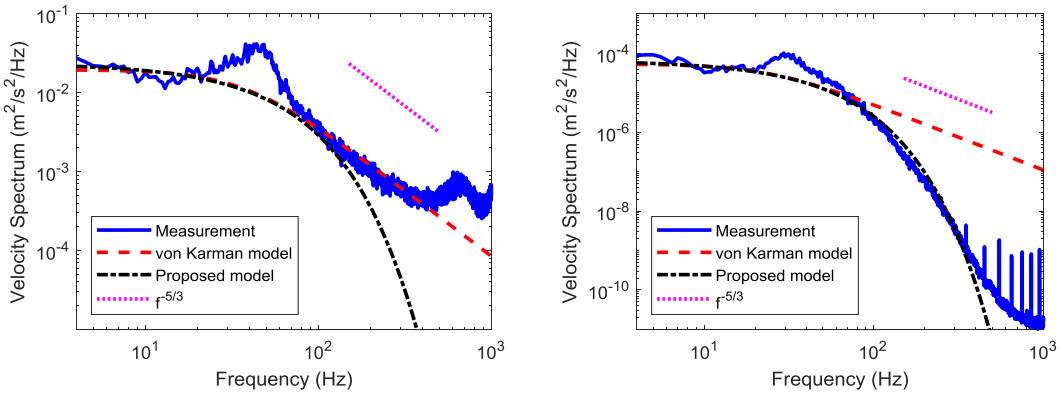

Fig. 2. (Color Online) Comparison of the von Karman-type model and the proposed model with the velocity spectrum measured (a) without and (b) with a 90 mm porous microphone windscreen at the mean wind speed of U = 5 m/s.

The reason for the difference between the velocity spectra in Figs. 2(a) and 2(b) is that the Reynolds number inside the porous windscreen was so small that the inertial range vanished. The velocity fluctuations were dramatically reduced by the porous windscreen, leading to a much smaller Reynolds number inside of the windscreen. For comparison, Table 1 summaries the characteristic velocity and length scale of the wind outside and inside of the porous windscreen, including the mean wind speed (U), the Root-Mean-Square (RMS) velocity (u_0), the Kolmogorov length scale (η), the Taylor microscale (λ) and the Taylor micrsoscale based Reynolds number (Re_λ). It is clear that both the RMS velocity and the Reynolds number inside of the porous windscreen were over 10 times smaller than that measured without the windscreen.

Table 1. Comparison of the characteristic velocity and length scale of the wind measured both with and without a 90 mm porous microphone windscreen.

	U (m/s)	u_0 (m/s)	η (m)	λ (m)	Re_λ
Without windscreen	5	1.3	9.6×10^{-5}	0.0032	277
With windscreen	0.40	0.08	3.2×10^{-4}	0.002	10

The wind noise spectra measured both with and without the porous windscreen are presented in Fig. 3, where the predictions are also shown for comparison. The exterior stagnation pressure (dashed line) and the exterior turbulence-turbulence interaction

pressure (dash-dot line) were calculated from Eqs. (2) and (3), respectively, based on the fitting constants that were obtained by fitting the von Karman-type model in Eq. (1) to the measured velocity spectrum in Fig. 2(a). The interior stagnation pressure (dotted line) was calculated from Eq. (6) based on the constants that were obtained by fitting Eq. (5) to the velocity spectrum measured inside the porous windscreen (Fig. 2(b)).

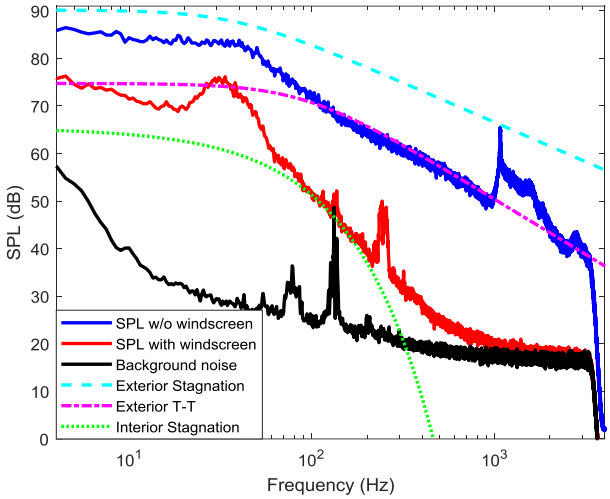

Fig. 3. Comparison of the measured and predicted wind noise spectra both with and without a porous microphone windscreen.

Figure 3 shows that the Sound Pressure Level (SPL) of the wind noise measured without the porous windscreen is slightly lower than the exterior stagnation pressure in the energy-containing range below the transition frequency (50 Hz). This is consistent with the outdoor measurement results by Raspet et al. (2008). However, in the inertial range above the transition frequency, the wind noise SPL was much lower than the exterior stagnation pressure, but agreed with the turbulence-turbulence interaction pressure instead. This is most likely because the small tube structure used to protect the hot-wire probe acts as a small windscreen to reduce the stagnation pressure on the microphone.

When the 90 mm diameter porous windscreen was installed, the wind noise SPL was reduced dramatically. In the energy-containing range below 10 Hz, the wind noise SPL inside the porous windscreen was well predicted by the turbulence-turbulence interaction pressure. This complies with the conclusion by Raspet et al. (2008) for outdoor wind noise, that the turbulence-turbulence (and the mean shear-turbulence)

241 interaction pressure would be measured by a perfect compact porous microphone
242 windscreen.
243 However, at higher frequencies, especially above the transition frequency (50 Hz),
244 the wind noise SPL inside the porous windscreen is much lower than the turbulence-
245 turbulence predictions based on the fitted von Karman-type model. Instead, the interior
246 stagnation pressure prediction, based on the proposed model fitted to the velocity
247 spectrum measured inside the windscreen, predicts the wind noise spectrum well
248 between 60 Hz and 200 Hz. For frequencies above 1000 Hz, the wind noise spectra
249 inside of the windscreen is almost the same as the background noise (measured when the
250 wind tunnel was off line).
251 Between 200 Hz and 1000 Hz, the wind noise spectrum is higher than the interior
252 stagnation prediction, indicating other wind noise sources. It is most likely caused by the
253 mean shear-turbulence interaction pressure that was not measured in this paper. There
254 are three potential sources for the mean shear-turbulence interaction in the wind tunnel
255 experiments. The first is the inherent shear in wind tunnel flows due to the limited size
256 of the nozzle. The flow speed decreases from the mean wind speed at the centerline of
257 the nozzle to zero far away from the nozzle. The other two sources for the mean shear is
258 the change in flow speed around the porous windscreen and the small tube structure. In
259 addition, the small tube structure may also introduce extra stagnation and turbulence-
260 turbulence interaction pressures that contribute to the wind noise spectra between 200
261 Hz and 1000 Hz. These potential wind noise sources will be investigated in future work.
262 The above results demonstrated that the wind noise inside porous windscreens
263 measured in wind tunnels showed different properties from that measured outdoors. The
264 conclusion drawn from the outdoor measurements, that a perfect windscreen can remove
265 the exterior stagnation pressure but cannot reduce the turbulence-turbulence interaction
266 pressure (Raspet et al., 2008), was valid only for the energy-containing range (low
267 frequency) in wind noise measured in wind tunnels, but not valid for the inertial range
268 (high frequency). In the inertial range, the stagnation pressure is easy to remove with a
269 simple structure around the microphone, such as the small tube structure used to protect
270 the hot-wire probe here, so that the wind noise spectrum degrades to the turbulence-
271 turbulence interaction pressure. When a porous windscreen was installed, the wind noise
272 was further reduced to much lower than the turbulence-turbulence interaction pressure.
273 The proposed model for the interior stagnation pressure was able to predict the wind
274 noise inside the windscreen between 60 Hz and 200 Hz, but underestimated the wind

noise level between 200 Hz and 1000 Hz, where other contributions might be dominant and needs further investigation.

It is noteworthy that the results here is not to show the conclusion for outdoor wind noise by Raspet et al. (2008) to be incorrect or inaccurate, but to present that the wind noise in porous windscreens measured in wind tunnels is different from that measured outdoors. When the wind speed is the same, the Reynolds number of wind tunnel flows is much smaller than that in the atmosphere due to the large turbulence scale of atmospheric winds (tens or hundreds of meters). The relatively small Reynolds number in wind tunnels makes the inertial range easier to convert to the dissipation range with the presence of porous materials. The specific difference between the indoor and outdoor wind noise inside porous windscreen needs further comparative investigations, which is the research topic of future work.

4. Conclusions

This paper investigated the wind noise spectra inside porous microphone windscreens with simultaneous measurements of wind velocity and pressure fluctuations in a wind tunnel. A velocity spectrum model was proposed to fit the wind velocity spectrum measured inside porous windscreen, based on which the interior stagnation pressure was calculated. It was found that in wind tunnel measurements, a porous windscreen reduced the wind noise to different levels at different frequency ranges. In the energy-containing range, the porous microphone windscreen reduced the wind noise from the exterior stagnation pressure to the turbulence-turbulence interaction pressure. In the inertial range, the porous windscreen further reduced the wind noise to much lower than the turbulence-turbulence interaction pressure. The lower frequency part of the inertial range was predicted well by the proposed interior stagnation pressure while the higher frequency part was dominant by other yet unknown noise source. Future work includes investigating the mean shear-turbulence interaction pressure in wind tunnel measurements and comparing the results with the mean shear-turbulence interaction pressure measured outdoors.

ACKNOWLEDGMENTS

This research was supported under National Key R&D Program of China (Grant No. 2017YFF0205006), National Natural Science Foundation of China (Grants Nos. 11934009, 11674173, 11874216 and 51575502), Jiangsu 333 High-level Talents

Training Project, Australian Research Council's Linkage Projects funding scheme (Grant No. LP140100740), and UTS FEIT Tech Lab Blue Sky Scheme.

References

Alamshah, V., Zander, A., and Lenchine, V. (**2015**). "Effects of turbulent flow characteristics on wind induced noise generation in shielded microphones," Proc. Acoust. 2015, 1–11. Retrieved from https://www.acoustics.asn.au/conference_proceedings/AAS2015/papers/p83.pdf

Lin, I.-C., Hsieh, Y.-R., Shieh, P.-F., Chuang, H.-C., and Chou, L.-C. (**2014**). "The effect of wind on low frequency noise," Proc. INTER-NOISE 2014, Melbourne, Australia, 1–12.

Lohse, D., and Muller-Groeling, A. (**1995**). "Bottleneck effects in turbulence: Scaling phenomena in r versus p space," Phys. Rev. Lett., **74**, 1747–1750. doi:10.1103/PhysRevLett.74.1747

Monin, A. S., and Yaglom, A. M. (**1965**). *Statistical fluid mechanics: mechanics of turbulence*, The MIT Press, Massachusetts, US, 887 pages.

Niu, F., Yang, P., Xu, H., He, L., Zhong, B., Bai, Y., and Feng, X. (**2017**). "Introduction of the small acoustic wind tunnel in NIM," Proc. INTER-NOISE 2017, HONG KONG, 1–4.

Pope, S. B. (**2000**). *Turbulent flows*, Cambridge University Press, New York, 771 pages.

Raspet, R., Webster, J., and Dillion, K. (**2006**). "Framework for wind noise studies," J. Acoust. Soc. Am., **119**, 834–843. doi:10.1121/1.2146113

Raspet, R., Yu, J., and Webster, J. (**2008**). "Low frequency wind noise contributions in measurement microphones," J. Acoust. Soc. Am., **123**, 1260–1269. doi:10.1121/1.2832329

Wang, L., Zander, A. C., and Lenchine, V. V (**2012**). "Measurement of the self-noise of microphone wind shields," Proc. 18th Australas. Fluid Mech. Conf. AFMC 2012, Launceston, Australia, 1–4.

Zhao, S., Cheng, E., Qiu, X., Burnett, I., and Liu, J. C. (**2017**). "Wind noise spectra in small Reynolds number turbulent flows," J. Acoust. Soc. Am., **142**, 3227–3233. doi:10.1121/1.5012740

Zhao, S., Cheng, E., Qiu, X., Burnett, I., and Liu, J. C. (**2018**). "Spatial decorrelation of wind noise with porous microphone windscreens," J. Acoust. Soc. Am., **143**, 330–339. doi:10.1121/1.5021335